Mon. Not. R. Astron. Soc. **394,** 2127–2140 (2009) doi:10.1111/j.1365-2966.2009.14474.x

Probing the age and structure of the nearby very young open clusters NGC 2244 and 2239

C. Bonatto[1⋆] and E. Bica[1⋆]

Departamento de Astronomia, Universidade Federal do Rio Grande do Sul Av. Bento Gonçalves 9500, Porto Alegre 91501-970, RS, Brazil

Accepted 2009 January 7. Received 2009 January 6; in original form 2008 December 1

ABSTRACT

The very young open cluster (OC) NGC 2244 in the Rosette Nebula was studied with field-star-decontaminated Two-Micron All-Sky Survey (2MASS) photometry, which shows the main-sequence (MS) stars and an abundant pre-MS (PMS) population. Fundamental and structural parameters were derived with colour–magnitude diagrams (CMDs), stellar radial density profiles (RDPs) and mass functions (MFs). Most previous studies centred NGC 2244 close to the bright K0V star 12 Monocerotis, which is not a cluster member. Instead, the near-infrared RDP indicates a pronounced core near the O5 star HD 46150. We derive an age within 1–6 Myr, an absorption $A_V = 1.7 \pm 0.2$, a distance from the Sun $d_\odot = 1.6 \pm 0.2$ kpc (≈1.5 kpc outside the solar circle), an MF slope $\chi = 0.91 \pm 0.13$ and a total (MS+PMS) stellar mass of $\sim$625 $M_\odot$. Its RDP is characterized by the core and cluster radii $R_c \approx 5.6$ arcmin (≈2.6 pc) and $R_{RDP} \approx 10$ arcmin (≈4.7 pc), respectively. Departure from dynamical equilibrium is suggested by the abnormally large core radius and the marked central stellar excess. We also investigate the elusive neighbouring OC NGC 2239, which is low mass ($m_{MS+PMS} \approx 301\,M_\odot$), young ($5 \pm 4$ Myr) rather absorbed ($A_V = 3.4 \pm 0.2$), and located in the background of NGC 2244 at $d_\odot = 3.9 \pm 0.4$ kpc. Its RDP follows a King-like function of $R_c \approx 0.5$ arcmin ≈ 0.5 pc and $R_{RDP} \approx 5.0$ arcmin ≈ 5.6 pc. The MF slope, $\chi = 1.24 \pm 0.06$, is essentially Salpeter's initial mass function. NGC 2244 is probably doomed to dissolution in a few 10^7 yr. Wide-field extractions and field-star decontamination increase the stellar statistics and enhance both CMDs and RDPs, which is essential for faint and bright star clusters.

Key words: open clusters and associations: general – open clusters and associations: individual: NGC 2244 – open clusters and associations: individual: NGC 2239.

1 INTRODUCTION

Still in the process of emerging from the parent molecular cloud, star clusters younger than about 5 Myr usually present a developing main sequence (MS) and a significant population of pre-MS (PMS) stars. However, depending on the initial cluster mass, star-formation efficiency and mass of the more massive stars, the rapid early gas removal (from supernovae and massive star winds) may impart important changes to the original gravitational potential. One consequence of the reduced potential is that stars, especially the low mass ones, moving faster than the scaled-down escape velocity may be driven into the field. Over a time-scale of 10–40 Myr, this effect can dissolve most of the very young star clusters (e.g. Goodwin & Bastian 2006). Indeed, estimates (e.g. Lada & Lada 2003) predict that only about 5 per cent of the embedded clusters are able to dynamically evolve into bound open clusters (OCs).

⋆E-mail: charles@if.ufrgs.br (BC); bica@if.ufrgs.br (EB)

On observational grounds, the dramatic changes in the potential affecting the early cluster spatial structure should be reflected on the stellar radial density profile (RDP). Bochum 1 (Bica, Bonatto & Dutra 2008a), for instance, can be an example of this scenario, in which the irregular RDP does not follow a cluster-like profile. This suggests significant profile erosion or dispersion of stars from a primordial cluster.

In the present paper, we address the case of NGC 2244 in the Rosette Nebula, which is also related to the Monocerotis OB2 association (e.g. Román-Zúñiga & Lada 2008). Historically, in colour–magnitude diagram (CMD) studies some authors centred the large-scale structure on 12 Mon, which is a bright foreground star of spectral type K0V. When only wide-field CMDs are considered, the adoption of this centre does not affect the results. However, as will be explored in this work in the context of investigating the cluster structure, that region is definitely at the cluster periphery.

Based on Shanghai Observatory plates with baselines of 34 and 87 yr, Chen, de Grijs & Zhao (2007) derived proper motions (PMs) and membership probabilities for NGC 2244. They found mass

segregation, but no velocity-mass dependence, indicating a primordial mass segregation related to the star-formation process. With arguments based on published initial mass functions (IMFs) and the measured internal velocity dispersion of $\approx 5\,\mathrm{km\,s^{-1}}$, they concluded that NGC 2244 will be dissolved on a short time-scale.

Additionally, in the area of the Rosette Nebula, the cluster candidate NGC 2239 has been frequently included in catalogues, but hardly studied. Both NGC 2244 and 2239 are optical clusters, while the area includes numerous infrared embedded clusters in the Rosette Molecular Cloud (e.g. Phelps & Lada 1997).

This work employs Two Micron All Sky Survey (2MASS)[1] near-infrared (NIR) J, H and K_s photometry. The 2MASS spatial and photometric uniformity allow extractions of wide surrounding fields that provide high star-count statistics. This property makes 2MASS an excellent resource to extract photometry of a broad variety of star clusters, the wide field ones in particular. For this purpose, we have been developing quantitative tools to statistically disentangle cluster evolutionary sequences from field stars in CMDs. Decontaminated CMDs have been used to investigate the nature of cluster candidates and derive their astrophysical parameters (e.g. Bica, Bonatto & Camargo 2008a). Basically, we apply (i) field-star decontamination to measure the statistical significance of the CMD morphology, which is fundamental to derive reddening, age and distance from the Sun, and (ii) colour–magnitude filters, which are essential for intrinsic stellar RDPs, as well as luminosity and mass functions (MFs). In particular, the use of field-star decontamination in the construction of CMDs has proved to constrain age and distance more than working with raw (observed) photometry, especially for low-latitude OCs (Bonatto et al. 2006a).

2MASS can be deep for nearby young or old OCs. For instance, our group has studied the young OCs NGC 6611 (Bonatto, Santos & Bica 2006c) and NGC 4755 (Bonatto et al. 2006b). Abundant pre-MS (PMS) stars were seen in the $\approx$1 Myr old NGC 6611, which is essentially embedded, and a few remaining ones in the $\approx$14 Myr old NGC 4755. As nearby older OCs we cite NGC 2477 (Bonatto & Bica 2005) and M 67 (Bonatto & Bica 2003).

In this paper, we apply our set of analytical tools to the 2MASS photometry of the stars in the area of NGC 2244 to derive its fundamental parameters, structure and fraction of MS and PMS stars. We also investigate the neighbouring cluster NGC 2239.

This paper is organised as follows. In Section 2, we recall literature data on NGC 2244. In Section 3, we describe the 2MASS photometry and compare it with the available optical data; we also describe the field-star decontamination algorithm and build CMDs. In Section 4, we derive cluster fundamental parameters. In Section 5, we derive structural parameters by means of stellar RDPs. In Section 6, we provide estimates of cluster mass. In Section 7, we compare the structural parameters and dynamical state of the present clusters with those of a sample of nearby OCs. Concluding remarks are given in Section 8.

2 PREVIOUS WORK ON NGC 2244

Several studies on NGC 2244, especially photometric and spectroscopic ones, are available in the literature.

The WEBDA[2] data base locates the cluster centre at $\alpha(2000) = 06^{\mathrm{h}}31^{\mathrm{m}}55^{\mathrm{s}}$ and $\delta(2000) = +04^{\circ}56'30''$, and provides a distance from the Sun $\mathrm{d}_{\odot} = 1.45$ kpc, reddening $E(B-V) = 0.46$ and an age of 7.9 Myr.

With UBV photometry, Ogura & Ishida (1981) obtained $E(B-V) = 0.47$, a total to selective extinction ratio $R_V = 3.2$, $\mathrm{d}_{\odot} = 1.42$ kpc, 4 Myr of age and a total mass of $5000\,\mathrm{M}_{\odot}$. With similar data, Hensberge, Pavlovski & Verschueren (2000) derived an age of 2 Myr, $R_V = 3.2 \pm 0.07$, $E(B-V) = 0.44$ and $\mathrm{d}_{\odot} = 1.4 \pm 0.1$ kpc.

In a comprehensive study of the Northern Monoceros region, Pérez (1991) found an apparent diameter of 24 arcmin, an age within 1.45 − 3.63 Myr, $\mathrm{d}_{\odot} = 1.67$ kpc, E(B − V) = 0.48 and a total mass of $770\,\mathrm{M}_{\odot}$ for NGC 2244.

Park & Sung (2002) found an average $E(B-V) = 0.47 \pm 0.04$, $R_V = 3.1 \pm 0.2$ and $\mathrm{d}_{\odot} = 1.66$ kpc. By comparing their photometric results with theoretical evolution models, they derived a main-sequence turnoff (MSTO) age of 1.9 Myr and a PMS age spread of about 6 Myr. The IMF slope calculated for the mass range $3.2 \lesssim m(\mathrm{M}_{\odot}) \lesssim 100$ is flat ($\chi = -0.3 \pm 0.1$).

Berghöfer & Christian (2002) used optical photometry of X-ray selected stars to estimate an isochrone age of 3 Myr, but significantly younger stars are detected.

Li (2005) provided updates on the nature of this young OC, including its central position, physical scale and stellar population. They found substructures in NGC 2244 with 2MASS, in particular a companion 6.6 pc west (in fact NGC 2239) of the NGC 2244 centre, and probably a major stellar aggregate resembling an arc in structure right below the core. Also, a disc fraction of 21 ± 3 per cent was estimated for members with masses above $0.8\,\mathrm{M}_{\odot}$.

In a Chandra study of NGC 2244, Wang et al. (2008) detected over 900 X-ray sources, 77 per cent of which having optical or FLAMINGOS NIR counterparts. Their X-ray-selected population is estimated to be nearly complete between 0.5 and $3\,\mathrm{M}_{\odot}$. The K-band luminosity functions (LFs) indicate a normal Salpeter (1955) IMF for NGC 2244, which differs from the top-heavy one reported in earlier optical studies that lacked a good census of $\lesssim 4\,\mathrm{M}_{\odot}$ stars. The X-ray LF indicates a population of ∼2000 stars with a spatial distribution strongly concentrated around the central O5 star, HD 46150. The other early O star, HD 46223, has few companions. The cluster's stellar RDP shows two structures: a power-law cusp around HD 46150 extending for ∼0.7 pc, surrounded by an isothermal sphere reaching out to 4 pc with core radius $R_{\mathrm{c}} = 1.2$ pc. This double structure, combined with the absence of mass segregation, indicates that NGC 2244 is not in dynamical equilibrium. The fraction of X-ray-selected members with K-band excesses caused by inner protoplanetary discs is 6 per cent, slightly lower than the 10 per cent disc fraction estimated from FLAMINGOS. The Rosette X-ray spectra of OB stars are soft and consistent with the standard model of small-scale shocks in the inner wind of a single massive star.

Recently, Román-Zúñiga & Lada (2008) reviewed the Rosette Complex, in particular they refer to the position of two OCs, NGC 2244 at position 'C' in the top-right panel of Fig. 1, and the other at position 'A', designated as NGC 2237. We call attention that their NGC 2244 actually is in the region of the original NGC 2239, while NGC 2237 refers to NGC 2244, near the position of HD 46150.

Román-Zúñiga & Lada (2008) build a scenario where an expanding H II region generated by a large OB association interacts with a giant molecular cloud, which harbours a number of embedded and OCs.

The wealth of papers on NGC 2244 reflects the complex – and, at the same time beautiful – nature of the interplay between bright massive stars, faint pre-MS stars and a thinning dust shroud, all

[1] The 2MASS, All Sky data release (Skrutskie et al. 1997), available at http://www.ipac.caltech.edu/2mass/releases/allsky/
[2] www.univie.ac.at/webda

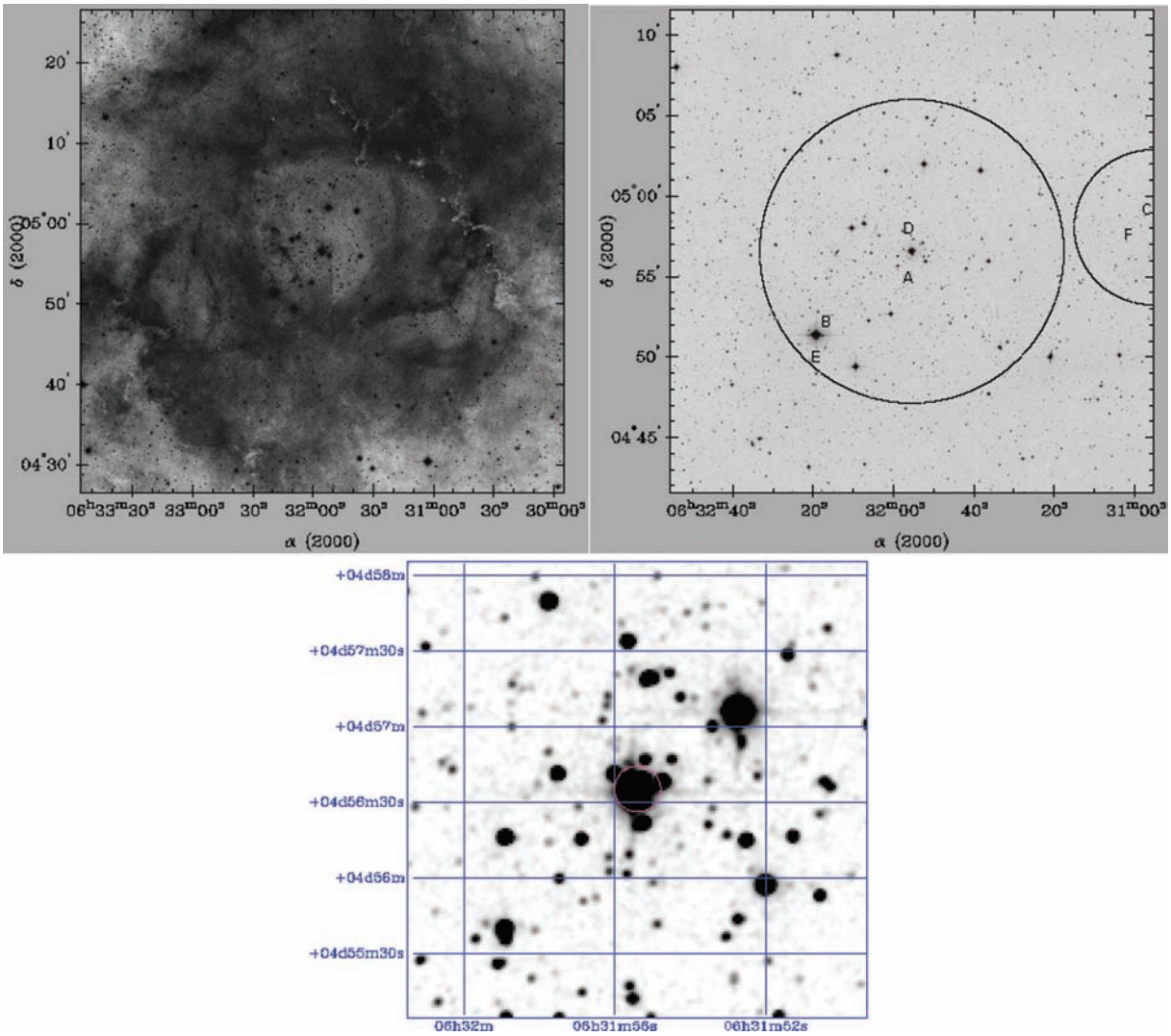

Figure 1. Top-left panel: $1^\circ \times 1^\circ$ DSS B image of NGC 2244 and the Rosette Nebula, centred on the coordinates of Table 1. Right-hand panel: 30×30 arcmin^2 I image of the same region; circles indicate the cluster radii (Section 5) of NGC 2244 (east) and NGC 2239 (west). Several centres adopted for these clusters are identified in the right-hand panel. The K0V star 12 Mon is indicated by position 'B'. Other positions as indicated by the keys in Table 1. Bottom: K_s image of NGC 2244 taken from the 2MASS Image Service focusing on the compact core within 3×3 arcmin^2. Same centre as in the B image. Orientation: north to the top and east to the left.

embodied in a single and relatively nearby object. Fig. 1 illustrates this scenario. In the Digitized Sky Survey (DSS)[3] B image (top-left panel) NGC 2244 emerges from the thin dust of the Rosette central part, which is also surrounded by strong gas emission. Indeed, gas emission and dust absorption are nearly absent in the XDSS I image (top-right), and especially in the 2MASS K_s image (bottom). Different centres adopted for NGC 2244 in previous (mostly optical) studies are indicated in the top-right panel. However, when seen in K_s, the cluster is highly concentrated on HD 46150 (bottom panel), suggesting a compact core. A similar centre for NGC 2244 had already been suggested by, for example Pérez, Thé & Westerlund (1987).

The different centres are summarized in Table 1, which shows some confusion in the identification of the actual centre of NGC 2244. As will be discussed in Section 5, we take as centre the coordinates that present the maximum stellar density (Fig. 11) computed within circles of 0.25 arcmin in radius, for MS and PMS stars taken isolately (Section 3.3). The resulting coordinates (Table 1) are similar to those given by WEBDA. The same procedure was applied to find the centre of NGC 2239 (Section 5).

3 NIR AND OPTICAL PHOTOMETRIES COMPARED

Since the Rosette Nebula reaches about 1°, it is interesting to compare large-scale properties of the optical data with those in the NIR.

2MASS J, H and K_s photometry was extracted in a wide circular field with VizieR.[4] The basic condition is that the extraction radius R_{ext} should be large enough to allow determination of the background level (Section 5). We used $R_{ext} = 80$ arcmin (NGC 2244) and

[3] Extracted from the Canadian Astronomy Data Centre (CADC), at http://cadcwww.dao.nrc.ca/

[4] http://vizier.u-strasbg.fr/viz-bin/VizieR?-source=II/246

Table 1. Previously adopted centres of NGC 2244 and 2239.

Cluster	α(2000) (hms)	δ(2000) (° ′ ″)	ℓ (°)	b (°)	Key	R (arcmin)	Reference
(1)	(2)	(3)	(4)	(5)	(6)	(7)	(8)
NGC 2237	06:31:58.5	+04:54:35.7	206.34	−2.07	A	–	Román-Zúñiga & Lada (2008)
NGC 2244	06:32:18.0	+04:52:00.0	206.42	−2.02	B	–	Sulentic & Tifft (1973)
NGC 2244	06:30:36.1	+04:58:50.6	206.12	−2.34	C	–	Román-Zúñiga & Lada (2008)
NGC 2244	06:31:55.0	+04:58:30.0	206.28	−2.06	D	–	WEBDA
NGC 2244/12 Mon†	06:32:19.2	+04:51:21.6	206.43	−2.02	E	∼24	SIMBAD
NGC 2244	06:31:55.4	+04:56:35.3	206.30	−2.07		∼10	This work
NGC 2239	06:30:54.0	+04:57:00.0	206.18	−2.29	F	∼18	Sulentic & Tifft (1973)
NGC 2239	06:30:57.3	+04:58:09.0	206.17	−2.27		∼5	This work

Notes. (†): 12 Mon as the centre of NGC 2244. Col. 7: cluster radius.

Table 2. Derived cluster structural parameters.

Cluster	σ_{bg} (* arcmin^{-2})	σ_0 (* arcmin^{-2})	R_c (arcmin)	R_{RDP} (arcmin)	δ_c	1 arcmin (pc)	σ_{bg} (* pc^{-2})	σ_0 (* pc^{-2})	R_c (pc)	R_{RDP} (pc)
(1)	(2)	(3)	(4)	(5)	(6)	(7)	(8)	(9)	(10)	(11)
NGC 2244†	1.53 ± 0.02	3.87 ± 0.65	5.6 ± 0.8	10.0 ± 2.0	3.5 ± 0.6	0.466	7.0 ± 0.4	17.8 ± 3.0	2.6 ± 0.4	4.7 ± 0.9
NGC 2244‡	0.12 ± 0.01	0.95 ± 0.43	1.2 ± 0.9	8.0 ± 1.0	9.2 ± 4.1	0.466	0.5 ± 0.1	4.4 ± 1.9	0.6 ± 0.4	3.7 ± 0.5
NGC 2244*	1.41 ± 0.09	3.61 ± 0.61	5.7 ± 0.8	12.0 ± 2.0	3.6 ± 0.6	0.466	6.5 ± 0.4	16.6 ± 2.8	2.7 ± 0.4	5.6 ± 0.9
NGC 2239†	1.90 ± 0.05	12.77 ± 4.77	0.5 ± 0.1	5.0 ± 1.0	7.7 ± 2.9	1.127	1.5 ± 0.1	10.0 ± 3.7	0.5 ± 0.1	5.6 ± 1.1

Notes. RDPs built considering separately the MS+PMS (†), MS (‡) and PMS (*). Core (R_c) and cluster (R_{RDP}) radii are given in angular and absolute units. Column (6): cluster/background density contrast parameter ($\delta_c = 1 + \sigma_0/\sigma_{bg}$), measured in the colour–magnitude filtered RDPs. Column (7): arcmin to parsec scale.

$R_{ext} = 30$ arcmin (NGC 2239), which are considerably larger than the respective cluster radii (Section 5 and Table 2). In the absence of significant differential absorption (Bonatto & Bica 2007a), wide extraction areas provide statistics for a consistent colour and magnitude characterization of field stars. For decontamination purposes, comparison fields were extracted within wide rings located beyond the cluster radii. As photometric quality constraint, the 2MASS extractions were restricted to stars (i) brighter than the 99.9 per cent Point Source Catalogue completeness limit[5] in the cluster direction and (ii) with errors in J, H and K_s lower than 0.1 mag. The 99.9 per cent completeness limits refer to field stars, and depend on Galactic coordinates. Fig. 2 (panel a) shows the distribution of uncertainties as a function of magnitude for the stars in the direction of NGC 2244. The fraction of stars with J, H and K_s uncertainties lower than 0.05 mag is ≈ 80, ≈70 and ≈60 per cent, respectively. We employ the relations $A_J/A_V = 0.276$, $A_H/A_V = 0.176$, $A_{K_S}/A_V = 0.118$ and $A_J = 2.76 \times E(J-H)$ (Dutra, Santiago & Bica 2002), with $R_V = 3.1$. They stem from the extinction curve of Cardelli, Clayton & Mathis (1989).

The available B and V photometry for NGC 2244 was taken from SIMBAD[6] within the same extraction radius as that used for 2MASS. As expected, the number of detected stars at a given radius in the optical is significantly lower than in the NIR (Fig. 2, panel b). Indeed, the ratio of the number of stars detected in the NIR to the optical N_{NIR}/N_{opt} increases with distance to the cluster centre, being $N_{NIR}/N_{opt} \approx 2$ for $R \lesssim 10$ arcmin (approximately the cluster region) and $N_{NIR}/N_{opt} \approx 24$ for $R \lesssim 80$ arcmin. Except for

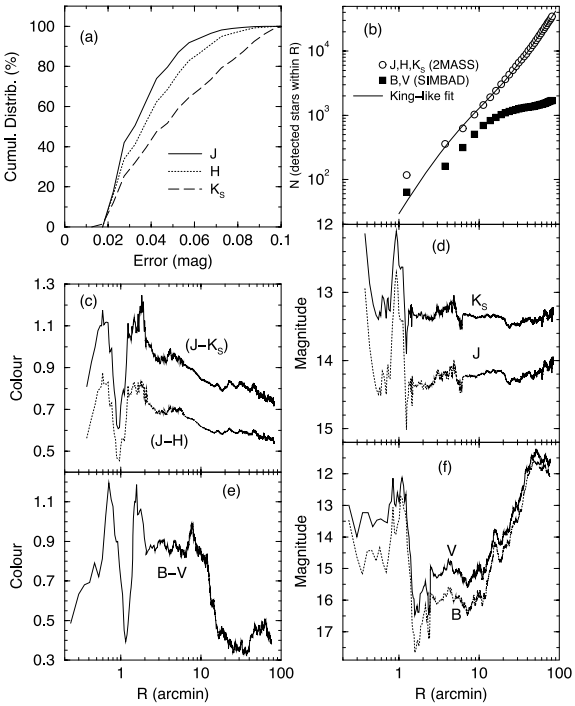

Figure 2. Panel (a): cumulative J, H and K_s photometric error distribution. (b): number of stars detected by 2MASS (empty circles) and SIMBAD (filled squares) within a given radius; except for the innermost bin, the 2MASS distribution follows a cluster-like profile (Section 5). (c) and (d): spatial dependence of the NIR colours and magnitudes. (e) and (f): same for the B and V bands.

[5] According to the 2MASS Level 1 Requirement, at http://www.ipac.caltech.edu/2mass/releases/allsky/doc/

[6] http://simbad.u-starsbg.fr/simbad

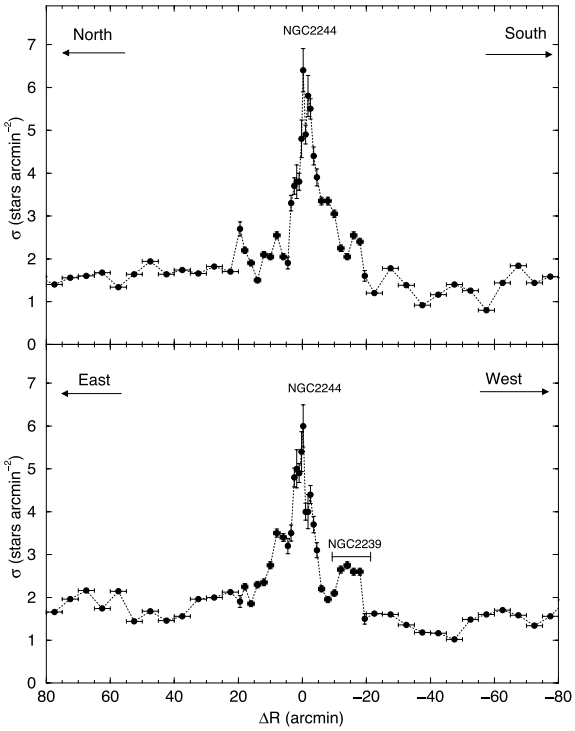

Figure 3. Linear extractions centred on NGC 2244. The extractions are 6 arcmin wide in both directions. The clusters are ≈15 arcmin apart along the east–west direction.

the innermost region, the stellar spatial distribution detected with 2MASS follows a cluster-like profile (Section 5), while the optical distribution deviates by a large amount (panel b). One conclusion is that analysis based on star counts in a dust-rich region is more realistic in the NIR than in the optical. Also, panel (b) shows that dust is thicker at large radii. This may have introduced biases in some of the previous optical studies.

The spatial dependence of the colours towards NGC 2244 is examined in Fig. 2 for the 2MASS (panel c) and optical (e) bands. The fiducial lines have been built as running averages of the raw (observed) data, with 10 points for $R < 2$ arcmin, 100 for $2 < R < 20$ arcmin and 1000 for $R > 20$ arcmin. Colours in both domains present a similar pattern, characterized by a blue core ($R \lesssim 2$ arcmin) containing essentially the MS stars. For larger radii, foreground stars dominate the optical photometry, while the NIR probes deeper regions. A similar effect occurs in the average magnitudes (panels d and f).

As suggested by the $\Delta R = 6$ arcmin linear extractions along the north–south and east–west directions (Fig. 3), a reasonable spatial uniformity level occurs with the 2MASS NIR photometry. Besides NGC 2244 itself, the next conspicuous bump is caused by NGC 2239 at ≈15 arcmin to the west. These profiles guided the comparison field selection.

Finally, in Fig. 4 (top panels), we show the spatial distribution of the stellar surface density (σ, in units of stars arcmin^{-2}) around NGC 2244, measured by 2MASS photometry. The surface density is computed in a rectangular mesh with cells of dimensions 2.5 × 2.5 arcmin^2, with meshes reaching total offsets of $|\Delta\alpha| = |\Delta\delta| \approx 20$ arcmin with respect to the centre (Table 1), in right ascension and declination. The respective isopleth surfaces are shown in the bottom panels, in which NGC 2239 shows up as a lower concentration at ≈15 arcmin to the west of NGC 2244. Two cases are considered

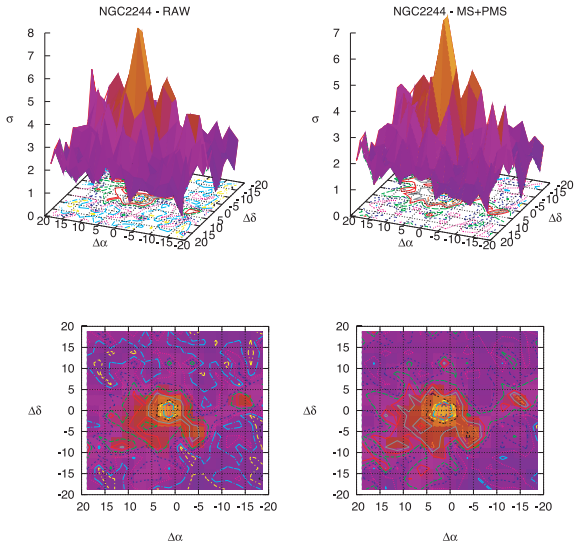

Figure 4. Top panels: stellar surface-density σ(stars arcmin^{-2}) of NGC 2244, computed for a mesh size of 2.5 × 2.5 arcmin^2, centred on the coordinates in Table 1. Bottom: the corresponding isopleth surfaces. Left-hand panel: observed (raw) photometry. Right-hand panel: MS and PMS stars selected by means of the colour–magnitude filter (Fig. 6). NGC 2239 shows up at ≈15 arcmin west of NGC 2244. $\Delta\alpha$ and $\Delta\delta$ in arcmin.

in Fig. 4, the observed (raw) photometry (left-hand panels) and the MS + PMS stars taken separately (right-hand panel) by means of a colour–magnitude filter (Section 3.3). Since an important fraction of the contaminant stars are excluded by the colour–magnitude filter, the surface density distribution of NGC 2244 (and NGC 2239) is better defined with respect to the surroundings.

3.1 Colour–magnitude diagrams with 2MASS photometry

CMDs displaying the $J \times (J - K_s)$ and $K_s \times (J - K_s)$ colours built with the raw photometry of NGC 2244 are shown in Fig. 6 (panels a and b). The sampled region ($R < 5$ arcmin) corresponds to about half of the cluster radius (Section 5). When qualitatively compared with the CMDs extracted from the equal-area comparison field (panels c and d), features typical of a very young OC emerge. A relatively vertical and populous MS [at $0.0 \lesssim (J - H), (J - K_s) \lesssim 0.3$] truncated for stars fainter than ≈12.5 (or mass $\lesssim 2.8\,M_\odot$ – Section 4) in both J and K_s, stand out over the field contamination.

3.2 Field decontamination

As expected of low-Galactic latitude clusters (Table 1), the stellar surface density in the direction of NGC 2244 (Fig. 4) confirms that the field-star contamination, including Mon OB2 and disc stars, should be taken into account. Further confirmation is provided by the qualitative comparison between the CMDs extracted within the cluster and field (Fig. 6). Obviously, the field contribution should be quantified for a better definition of the intrinsic CMD morphology.

Although difficult, decontamination is a very important step in the identification and characterization of star clusters. Most of the different approaches (e.g. Mercer et al. 2005) are based essentially on two different premises. The first relies on spatial variations of the star-count density, but does not take into account CMD evolutionary sequences. Alternatively, stars of an assumed cluster CMD are subtracted according to similarity of colour and magnitude with

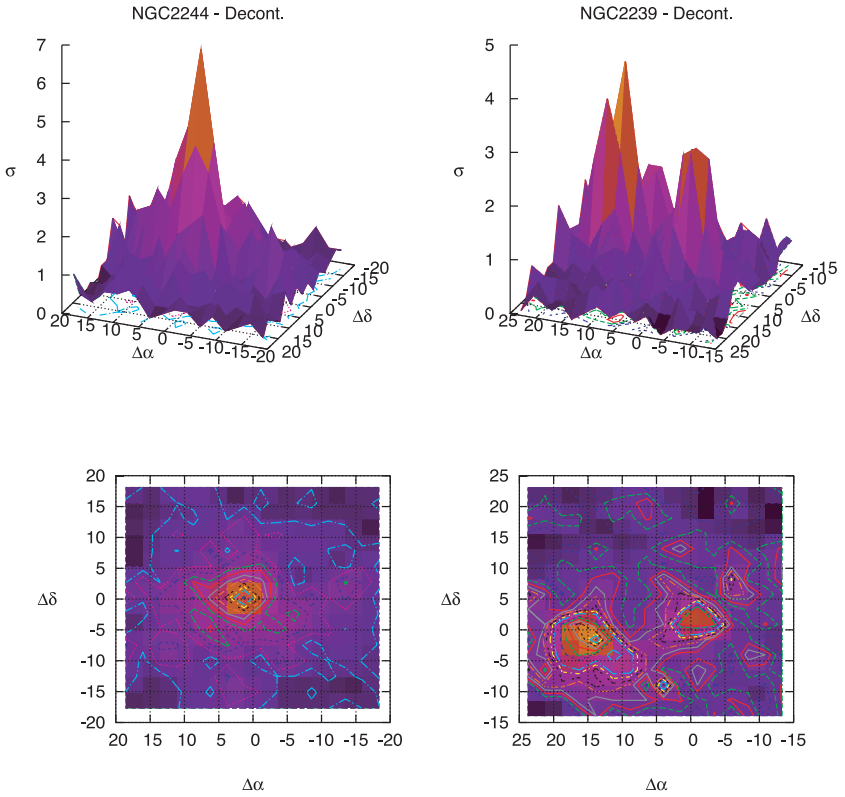

Figure 5. Similar to Fig. 4 for the decontaminated photometries of NGC 2244 (left-hand panels) and NGC 2239 (right-hand panel). NGC 2239 is the concentration ≈15 arcmin to the west of the prominent NGC 2244.

the stars of an equal-area comparison field CMD. Together with the present one, these methods are based on photometric properties only. Ideally, more robust results on membership determination would be obtained if another independent parameter, such as the PM of member and comparison field stars, is taken into account. However, for PM to be useful the cluster should be relatively nearby (e.g. Alessi, Moitinho & Dias 2003) and/or to have been observed in widely apart epochs preferentially with high resolution, as for the globular cluster (GC) NGC 6397 (Richer et al. 2008). Neither condition is fully satisfied for NGC 2244, which is relatively distant (Section 4) and was observed by 2MASS in a single epoch. As a consequence, only about 50 per cent of the stars within $R = 10$ arcmin of NGC 2244 have optical PM measured (Section 3.4).

Our decontamination algorithm is fully described in Bonatto & Bica (2007a), Bica et al. (2008a) and Bica & Bonatto (2008). For clarity, we provide here only a brief description. The algorithm measures the relative number densities of probable field and cluster stars in cubic CMD cells with axes along the J magnitude and the $(J - H)$ and $(J - K_s)$ colours. It (i) divides the full range of CMD magnitude and colours into a 3D grid, (ii) estimates the number density of field stars in each cell based on the number of comparison field stars with similar magnitude and colours as those in the cell and (iii) subtracts the expected number of field stars from each cell. Input algorithm parameters are the cell dimensions $\Delta J = 1.0$ and $\Delta(J - H) = \Delta(J - K_s) = 0.2$; the comparison fields are located within $R = 30 - 80$ arcmin (NGC 2244) and $R = 20 - 30$ arcmin (NGC 2239). The equal-area field extractions (Figs 6 and 7) should be considered only for qualitative comparisons. The decontamination itself uses the large surrounding area as described above. Among other statistical tests, decontaminated CMDs of star clusters have integrated $N_{1\sigma} \gg 1$ (Bica et al. 2008a; Bica & Bonatto 2008), a condition that is fully met for the present objects, with $N_{1\sigma} = 13.0, 6.5$, respectively for NGC 2244 and 2239.

3.2.1 *Decontaminated surface densities and CMDs*

We take the decontaminated surface-density distributions (Fig. 5) as an efficiency indicator. For the present clusters, the central excesses have been significantly enhanced with respect to the raw photometry (Fig. 4), while the residual surface density around the centre has been reduced to a minimum level. By design, the decontamination depends essentially on the colour–magnitude distribution of stars located in different spatial regions. The fact that the decontaminated surface density presents a conspicuous excess only at the assumed cluster position implies significant differences among this region and the comparison field, both in terms of colour–magnitude and number of stars within the corresponding colour–magnitude bins. This meets cluster expectations, which can be characterized by a single-stellar population, projected against a Galactic stellar field.

The decontaminated CMDs are shown in the bottom panels of Figs 6 and 7. As expected, essentially all contamination is removed, leaving stellar sequences typical of mildly reddened young OCs, with a well-developed MS and a significant population of PMS stars, especially in NGC 2244.

Although in both cases the MS width is rather tight and appears to be dominated by photometric errors, we cannot exclude the possibility of differential reddening to account for part of the observed spread, especially towards faint stars. To examine this issue we show, in Figs 6 and 7 (panels e and f), reddening vectors computed with the 2MASS ratios (Section 3.1) for a visual absorption $A_V = 2$, approximately the absorption derived for NGC 2244 and 2239 (Section 4). Together with the decontaminated CMDs, this

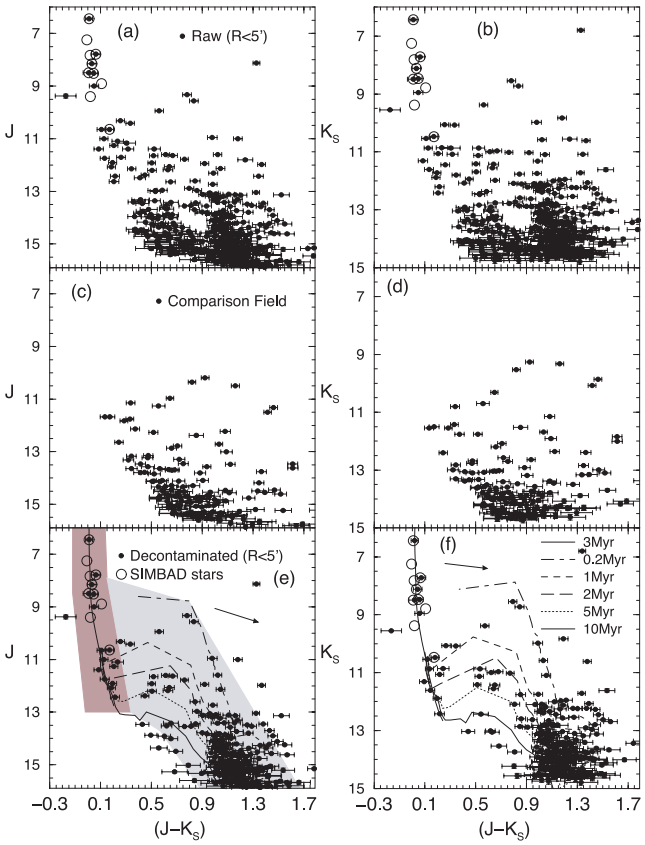

Figure 6. 2MASS CMDs of NGC 2244. Top panels: observed photometry extracted from the $R < 5$ arcmin region. Middle: equal-area comparison field CMDs, extracted within $29.58 < R < 30$ arcmin, including the Mon Ob2 association and disc contamination. Bottom panels: decontaminated CMDs with the MS fitted by the 3 Myr solar-metallicity Padova isochrone. PMS tracks of different ages are shown. The shaded polygons correspond to the MS (dark-gray) and PMS (light-gray) colour–magnitude filters (Section 3.3). The bright stars listed in SIMBAD are identified as circles; four of these are within $5 \lesssim R(\text{arcmin}) \lesssim 10$. Arrows in the bottom panels show the reddening vector computed for $A_V = 2$.

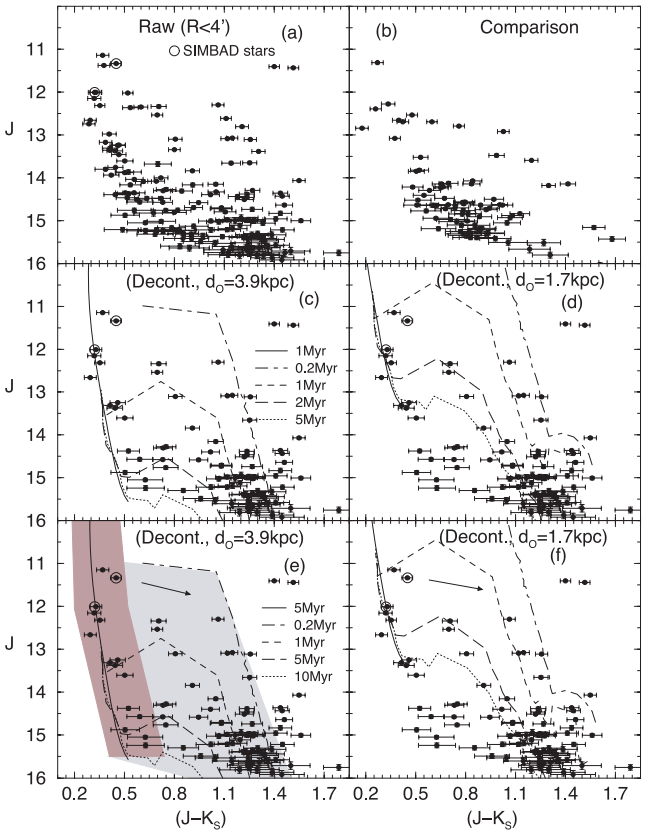

Figure 7. Similar to Fig. 6 for the region $R < 4$ arcmin (panel a) of NGC 2239, and the equal-area comparison field (b). Panels (c)–(f): decontaminated CMD with different age/distance from the Sun solutions. Bright stars with SIMBAD optical data are indicated as open circles. Arrows show the reddening vector computed for $A_V = 2$.

experiment shows that differential reddening in both clusters is not significant.

We conclude that the qualitative and quantitative expectations of the decontamination algorithm have been satisfied by the output. In both cases, the decontaminated photometry presents a relevant excess, with respect to the surroundings, in the surface-density distribution (Fig. 5). In addition, field-decontaminated CMDs extracted from the spatial regions where the excesses occur (Figs 6 and 7), present statistically significant cluster CMDs.

3.3 Colour–magnitude filters

To minimize CMD noise, we apply colour–magnitude filters to the raw photometry to exclude stars with colours unlike those of the cluster sequence. The filters are wide enough to include cluster MS stars and the 1σ photometric uncertainties.[7] For very young OCs such as NGC 2244 and 2239, we also include filters to account for the PMS population. The colour–magnitude filters for the present OCs are shown in Figs 6 and 7.

3.4 Proper motions

Another indication of the star cluster nature of NGC 2239 is provided by NOMAD[8] PM data taken for the stars extracted within the same spatial region as the 2MASS data. However, the correspondence between NOMAD and 2MASS detections is not complete, with ≈50 per cent of the stars detected with 2MASS included in NOMAD, for the colour–magnitude filtered photometry of both NGC 2244 and 2239.

In Fig. 8, we show histograms of the right ascension (μ_α cos (δ)) and declination (μ_δ) PM components measured for the member+field and field stars. We use the same cluster and comparison field extractions as those defined for the decontamination process (Section 3.2). The field histograms have been normalized to match the cluster projected area. Finally, the intrinsic PM distributions are obtained by subtracting the normalized field histogram from that of the field+members.

[7] Colour–magnitude filter widths should also account for formation or dynamical evolution-related effects, such as enhanced fractions of binaries (and other multiple systems) towards the central parts of clusters, since such systems tend to widen the MS (e.g. Hurley & Tout 1998; Kerber et al. 2002; Bonatto, Bica & Santos 2005; Bonatto & Bica 2007a).

[8] http://vizier.u-strasbg.fr/viz-bin/VizieR?-source=I/297. NOMAD is based on the International Celestial Reference System (ICRS) with origin at the Solar system barycentre.

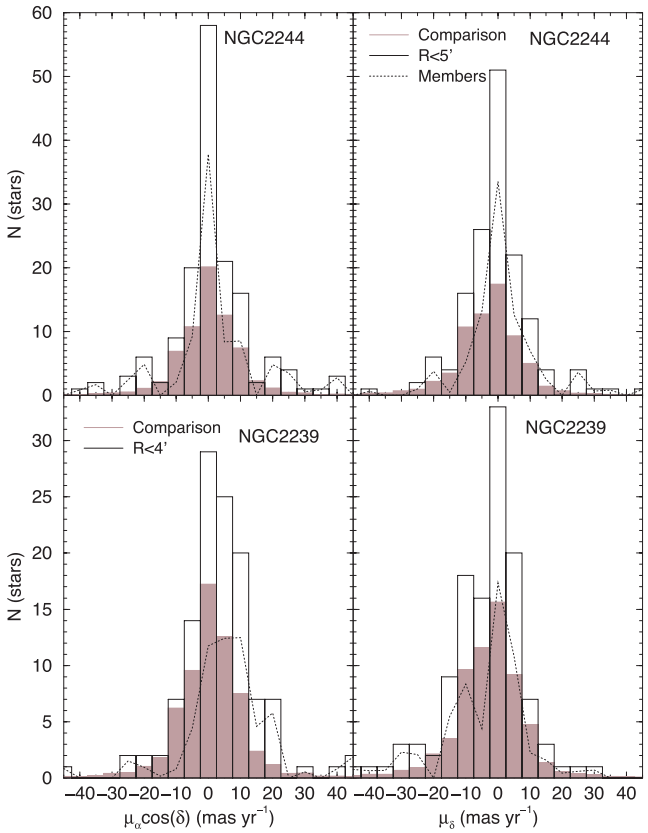

Figure 8. Comparative histograms of the member+field (white) and comparison field stars (shaded), which were scaled to match the projected areas. The intrinsic distributions are shown by the dashed lines for the extraction $R < 5$ arcmin of NGC 2244 (top panels) and $R < 4$ arcmin of NGC 2239 (bottom).

Both NGC 2244 and 2239 present conspicuous PM excesses over the field. As expected of an OC, the intrinsic PM distribution of NGC 2244 (Fig. 8, top panels) is essentially Gaussian. Although somewhat less defined, a similar conclusion applies to NGC 2239 (bottom panels). Besides, NGC 2244 shares essentially the same motion as the disc-field/Mon OB2 association, which is consistent with a relatively nearby OC. NGC 2239, on the other hand, appears to be located at a different distance, especially because of the significant shift in μ_α cos (δ) between member and field stars.

4 CLUSTER AGE, REDDENING AND DISTANCE

The field-decontaminated CMD morphologies (Section 3.1) can be used to compute cluster fundamental parameters. Both NGC 2244 (Fig. 6) and 2239 (Fig. 7) present MS and PMS stars that can be used as constraints. We adopt solar-metallicity isochrones because the clusters are young and not far from the solar circle (see below), a region essentially occupied by [Fe/H] $\approx$ 0.0 OCs (Friel 1995).

To deal with the MS, we use Padova isochrones (Girardi et al. 2002) computed with the 2MASS J, H and K_s filters.[9] The tracks of Siess, Dufour & Forestini (2000) are used to characterize the PMS distributions.

We take $R_\odot = 7.2 \pm 0.3$ kpc (Bica et al. 2006) as the Sun's distance to the Galactic Centre to compute Galactocentric distances, a value derived by means of the GC spatial distribution.[10]

Historically, different approaches have been used to extract astrophysical parameters from isochrone fits. The simplest ones are based on a direct comparison of a set of isochrones with the CMD morphology, while the more sophisticated ones include photometric uncertainties, binarism and metallicity variations. Most of these methods are summarized in Naylor & Jeffries (2006), in which a maximum-likelihood CMD fit method is described. We caution that, because of the 2MASS photometric uncertainties for the lower sequences, a more sophisticated approach for isochrone fitting might lead to an overinterpretation.

For the above reasons, fits are made *by eye*, with the MS and PMS stellar distributions as constraint. We also require that, because of the probable presence of binaries, the adopted (single-star) MS isochrone should be shifted somewhat to the left of the MS fiducial line, that is a median line that takes into account the MS spread, including the photometric uncertainties as well (e.g. Bonatto et al. 2005, and references therein). In the following, we discuss the present clusters individually.

4.1 NGC 2244

The decontaminated CMD morphology of NGC 2244 (Fig. 6) shows a nearly vertical MS at $J \lesssim 13$ and $0.0 \lesssim (J - K_s) \lesssim 0.4$, and a population of low-mass PMS stars at $J \gtrsim 13.5$ and $0.9 \lesssim (J - K_s) \lesssim 1.5$. Taken together, these stellar sequences unambiguously characterize a very young OC.

Allowing for photometric uncertainties, acceptable fits to the decontaminated MS morphology are obtained with any isochrone with age in the range 1–6 Myr. The PMS stars in Fig. 6 are basically contained within the 0.2 and 6 Myr PMS isochrones (Siess et al. 2000), thus implying a similar age range as the MS. Accordingly, we take the 3 Myr isochrone as representative solution.

With the adopted solution, the fundamental parameters of NGC 2244 are a NIR reddening $E(J-H) = 0.17 \pm 0.02$ [or $E(B-V) = 0.54 \pm 0.06$ and $A_V = 1.7 \pm 0.2$], an observed and absolute distance moduli $(m-M)_J = 11.5 \pm 0.2$ and $(m-M)_O = 11.03 \pm 0.21$, respectively, and a distance from the Sun $d_\odot = 1.6 \pm 0.2$ kpc. Thus, for $R_\odot = 7.2$ kpc, the Galactocentric distance of NGC 2244 is $R_{GC} = 8.7 \pm 0.2$ kpc, which puts it $\approx$1.5 kpc outside the Solar circle. This solution is shown in Fig. 6 (panels e and f). The age spread indicates a non-instantaneous star formation process, similar to what was found for, for example NGC 4755 (Bonatto et al. 2006b) and NGC 6611 (Bonatto et al. 2006c).

4.2 NGC 2239

Although somewhat less populated than NGC 2244, the decontaminated CMD of NGC 2239 also presents MS and PMS sequences (Fig. 7), which suggests a similar age as that of NGC 2244. However, this less-constrained CMD admits alternative age/distance solutions.

[9] http://stev.oapd.inaf.it/cgi-bin/cmd. These isochrones are very similar to the Johnson–Kron–Cousins ones (e.g. Bessel & Brett 1988), with differences of at most 0.01 in colour (Bonatto, Bica & Girardi 2004).

[10] Other recent studies gave similar results, e.g. $R_\odot = 7.2 \pm 0.9$ kpc (Eisenhauer et al. 2003), $R_\odot = 7.62 \pm 0.32$ kpc (Eisenhauer et al. 2005) and $R_\odot = 7.52 \pm 0.10$ kpc (Nishiyama et al. 2006), with different approaches.

Thus, before the CMD fit, we compute the distance of the central bright stars projected on NGC 2239. We found two bright stars in SIMBAD in common with the 2MASS detections. These are the A 2 star GSC 00154−01659 ($B = 13.32$, $V = 12.90$, $J = 11.336$) and the B 5 star GSC 00154−02384 ($B = 13.42$, $V = 13.21$, $J = 12.014$). With the typical colours and magnitudes of stars given in Binney & Merrifield (1998), the A 2 star would be located at $d_\odot = 1.4$ kpc, while the B 5 would be at $d_\odot = 4.3$ kpc.

Together with young MS and PMS isochrones, both distances are used as starting point to search for fundamental parameters. The possible solutions are summarized in Fig. 7, for both the far (left-hand panels) and near (right-hand panel) distances. We consider the MS ages of 1 Myr (middle panels) and 5 Myr (bottom). The best fit for these ages was for $d_\odot \approx 3.9 \pm 0.4$ kpc and $d_\odot \approx 1.7 \pm 0.3$ kpc. Within uncertainties, they are consistent with those derived for the bright stars. The MS+PMS solutions for $d_\odot \approx 3.9$ kpc (Fig. 7, panels c and f) appear to account for essentially all of the decontaminated CMD sequences. Irrespective of age, the near solutions, on the other hand, fail to explain several faint stars below the MS.

Considering all available morphological and photometric properties, the best overall CMD fit (Fig. 7, panel e) corresponds to an age 5 ± 4 Myr, $E(J-H) = 0.34 \pm 0.02$, $E(B-V) = 1.10 \pm 0.06$, $A_V = 3.4 \pm 0.2$, $(m-M)_J = 13.9 \pm 0.2$, $(m-M)_O = 12.95 \pm 0.21$, $d_\odot = 3.9 \pm 0.4$ kpc and $R_{GC} = 10.8 \pm 0.3$ kpc, thus ≈3.6 kpc outside the solar circle. Thus, the B 5 star GSC 00154−01659 is probably a cluster member, while the A 2 star GSC 00154−01659 is probably in the foreground. We conclude that NGC 2239 lies ≈2.3 kpc in the background of NGC 2244.

4.3 Colour–colour diagrams

When transposed to the NIR colour–colour diagrams $(J - K_s) \times (H - K_s)$, the age and reddening solutions of NGC 2244 and 2239 derived above consistently match the field-star decontaminated photometry of these OCs (Fig. 9, left-hand panels). Since they include PMS stars, we use tracks of Siess et al. (2000) to characterize the age of NGC 2244 (∼3 Myr) and NGC 2239 (∼5 Myr). MS stars lie on the blue side of the diagram. Interestingly, only a low fraction of the stars of these OCs appears to be very reddened. In both cases, the distribution suggests a low fraction of disc stars, consistent with the estimates in the range 6–10 per cent (Wang et al. 2008).

4.4 The fraction of PMS and MS stars

Right after formation, most of a cluster's mass is stored in the PMS stars that, eventually, shed the dust layers and emerge into the MS (Section 1). Thus, the number of MS and PMS stars evolve in opposite directions with cluster age, till all stars are in the MS after about 30 Myr (Bonatto et al. 2006b, and references therein). Indeed, NGC 2244 and 2239 present different fractions of MS and PMS stars (Figs 6 and 7), which is consistent with the different ages.

To further explore this issue, we compute the ratio of the number of PMS to MS stars $f_{PMS/MS} = n_{PMS}/n_{MS}$. Then we examine the age dependence of $f_{PMS/MS}$ for the very young OCs, located at a similar distance as NGC 2244, studied by our group with the same methods as those employed in NGC 2244 and 2239. These conditions are satisfied by NGC 6611[11] (1.3 ± 0.3 Myr, $d_\odot \approx 1.8$ kpc – Bonatto et al. 2006c), Bochum 1 (9 ± 3 Myr, $d_\odot \approx 2.0$ kpc – Bica et al. 2008b) and NGC 4755 (14 ± 4 Myr, $d_\odot \approx 1.8$ kpc – Bonatto et al. 2006b).

[11] For consistency with the remaining clusters, we counted the number of PMS stars brighter than $J = 16$ in NGC 6611, since in Bonatto et al. (2006c) we restricted them to $J \leq 15$.

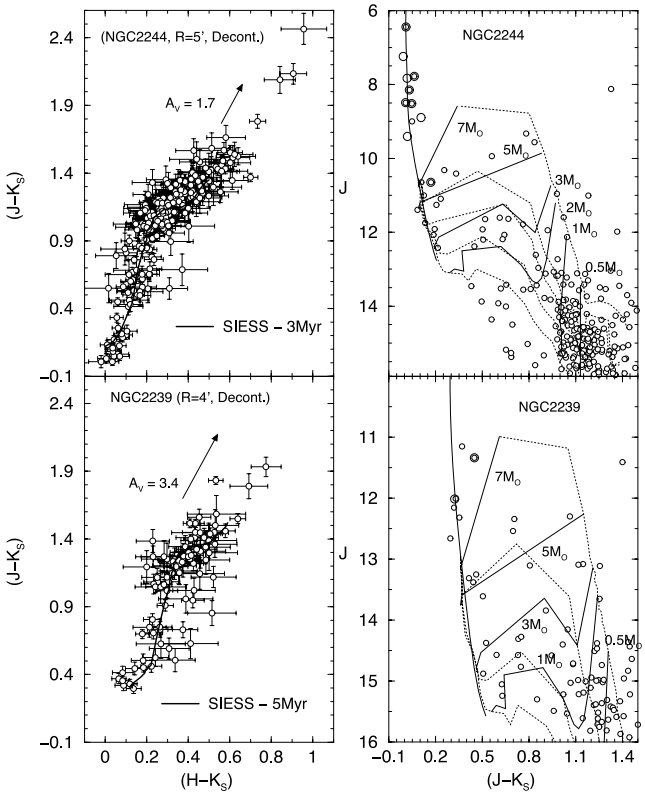

Figure 9. Colour–colour diagrams with the decontaminated photometry of NGC 2244 (top-left panel) and NGC 2239 (bottom-left). The 3 and 5 Myr Siess et al. (2000) isochrones, set with the derived reddening values, are used to show the PMS and MS sequences simultaneously. Reddening vectors for $A_V = 1.7$, 3.4 are shown for NGC 2244 and 2239, respectively. Right-hand panels: evolutionary tracks of PMS stars of different masses are superimposed on the decontaminated CMDs of NGC 2244 (top) and NGC 2239 (bottom).

Despite the considerable uncertainties in the age and the relatively small number of clusters, the $f_{PMS/MS}$ ratios shown in Fig. 10 appear to be consistent with the expected trend with cluster age. Indeed, we found that the ratios follow the exponential-decay function $f_{PMS/MS} \propto e^{-(age/\tau)}$, with the time-scale $\tau = 5.6 \pm 1.6$ Myr. Thus, it would take less than about 30 Myr for a cluster to retain only ≈5 per cent (a typical Poisson fluctuation) of the original PMS stars. It would be interesting to check this trend – and the above time-scale – for a statistically significant sample of young clusters, so that other parameters, such as cluster mass, and environmental effects can be considered as well.

5 CLUSTER STRUCTURE

We use the projected stellar RDPs, defined as the stellar number density around the cluster centre, to derive structural parameters. To minimize noise, we work with colour–magnitude filtered photometry to isolate the MS and PMS stars, which enhances the RDP contrast relative to the background, especially in crowded fields (e.g. Bonatto & Bica 2007a). However, field stars with colours similar to those of the cluster are expected to remain inside the colour–magnitude filter, affecting the intrinsic RDP in a way that depends

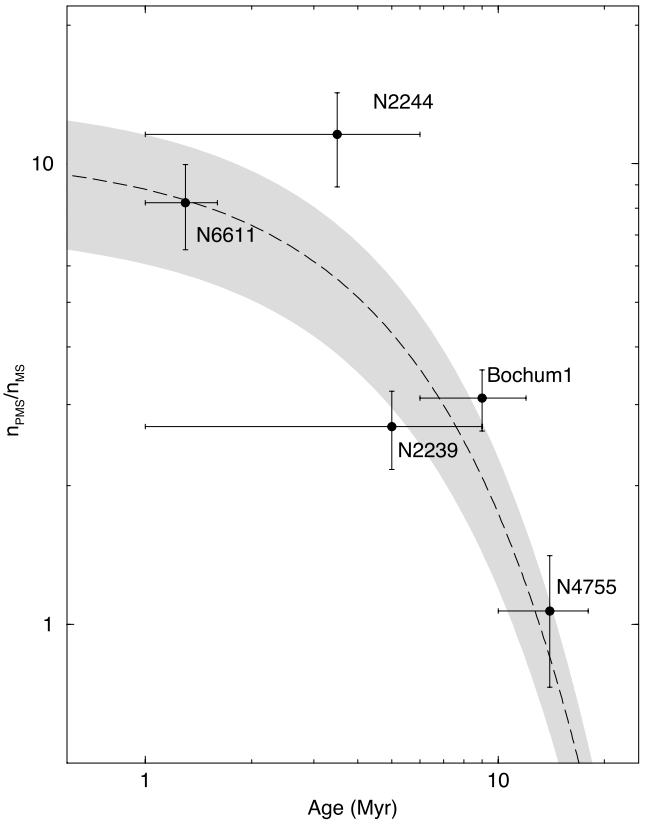

Figure 10. The ratio of the number of PMS to MS stars follows an exponential-decay function (dashed line) with cluster age: $n_{\rm PMS}/n_{\rm MS} \propto \exp(-{\rm age}/\tau)$, with $\tau = 5.6 \pm 1.6$ Myr. Fit uncertainties (1σ) are within the shaded region.

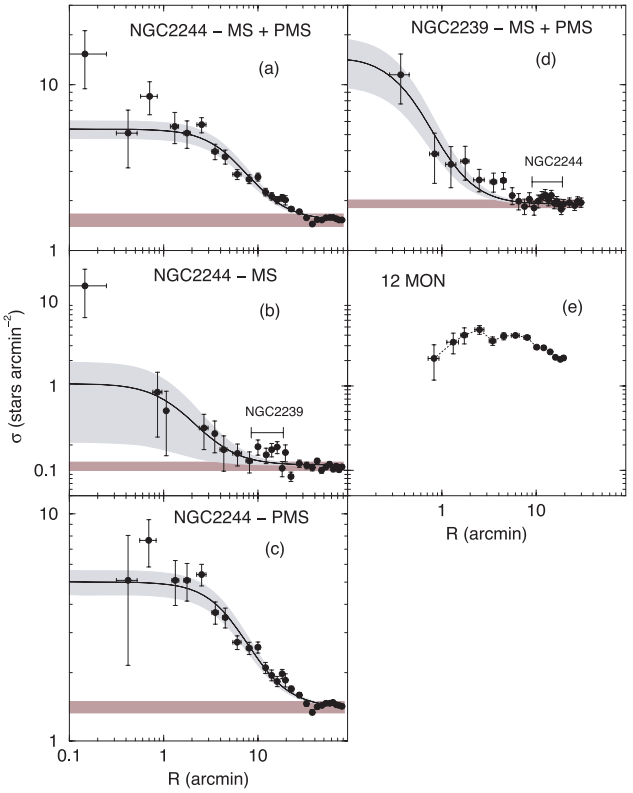

Figure 11. Stellar RDPs built with colour–magnitude filtered photometry. Solid line: best-fitting King-like profile. Horizontal shaded polygon: background. Shaded regions: 1σ King fit uncertainty. Note the central density excess in the RDP of NGC 2244 in panels (a) and (b). The RDP with 12 Mon as centre in shown in (d).

on the relative densities of field and cluster stars. The contribution of the residual contamination to the observed RDP is statistically evaluated by means of its extension into the field.

Rings of increasing width with distance from the cluster centre are built to avoid oversampling near the centre and undersampling at large radii. The set of ring widths used is $\Delta R = 0.25$, 0.5, 1.0, 2.0 and 5 arcmin, respectively, for $0 \leq R < 0.5$ arcmin, $0.5 \leq R < 2$ arcmin, $2 \leq R < 5$ arcmin, $5 \leq R < 20$ arcmin and $R \geq 20$ arcmin. The residual background level of each RDP corresponds to the average number-density of filtered field stars. The R coordinate (and uncertainty) of each ring corresponds to the average position and standard deviation of the stars inside the ring.

The colour–magnitude filtered RDPs of the clusters are shown in Fig. 11. As expected, minimization of the number of non-cluster stars by the colour–magnitude filter resulted in RDPs with a high contrast relative to the background. For NGC 2244, we also show the RDPs built with the MS and PMS stars separately (left-hand panels). Interestingly, while the MS RDP (panel b) has a conspicuous density excess for $R \approx 0.15$ arcmin, the PMS stars (panel c) are found only for $R \gtrsim 0.4$ arcmin. The presence of NGC 2239 causes a bump in the MS RDP of NGC 2244 (panel b). Similarly, NGC 2244 shows up in the RDP of NGC 2239 (d). Fig. 11 also shows the RDP produced with the star 12 Mon as centre (panel d). It is clear that 12 Mon cannot be the centre of NGC 2244.

Most star clusters have RDPs that follow a well-defined analytical profile for example the empirical, single mass, modified isothermal spheres of King (1966) and Wilson (1975),[12] and the power law with a core of Elson, Fall & Freeman (1987). Each function is characterized by a different set of parameters that are related to cluster structure. For simplicity and considering the error bars of the RDPs in Fig. 11, we adopt the function $\sigma(R) = \sigma_{\rm bg} + \sigma_0/[1 + (R/R_{\rm c})^2]$, where $\sigma_{\rm bg}$ is the residual background density, σ_0 is the central density of stars, and $R_{\rm c}$ is the core radius. It is similar to the function introduced by King (1962) to describe the surface brightness profiles in the central parts of GCs. To minimize degrees of freedom, σ_0 and $R_{\rm c}$ are obtained from the fit, while $\sigma_{\rm bg}$ is measured in the field. The RDP bins corresponding to the neighbouring clusters were ignored in the fit. The best-fitting solutions are shown in Fig. 11, and the parameters are given in Table 2. For absolute comparison with other clusters, Table 2 gives parameters in absolute units. Within uncertainties, the adopted King-like function describes well the colour–magnitude filtered RDP of NGC 2239 (panel d) along the full radius range. The same applies only for $R \gtrsim 1$ arcmin for the RDP of NGC 2244. The innermost bin in the MS (and to a lesser degree to the MS+PMS) RDP (panel b) presents a several σ excess over the fit. This RDP cusp basically corresponds to the detached grouping of stars (with a diameter of ≈0.25 arcmin) around HD 46150, seen in Fig. 1 (bottom-right panel). Our inner RDP shape agrees with that derived by Wang et al. (2008) with FLAMINGOS. In old star clusters, such a central RDP excess can be attributed to a post-core collapse, like those detected in some GCs

[12] It assumes a pre-defined stellar distribution function and produces more extended envelopes than King (1966).

(e.g. Trager, King & Djorgovski 1995). It has been detected as well in Gyr-class OCs, such as, for example NGC 3960 (Bonatto & Bica 2006) and LK 10 (Bonatto & Bica 2009). Another very young cluster harbouring such a detached core producing an RDP central cusp is NGC 6823 (Bica et al. 2008b). Clusters are not expected to dynamically evolve into a post-core collapse on short time-scales, and the cusp must have been caused by star-forming effects. The compact core within the eroded profile of Bochum 1 (Bica et al. 2008b) can be a long-lived structure in young clusters. Consequently, this central cusp in such a young cluster as NGC 2244 suggests a significant deviation from dynamical equilibrium (Section 7).

We also estimate the cluster radius ($R_{\rm RDP}$) by visually comparing the cluster RDP and background levels, i.e. $R_{\rm RDP}$ is the distance from the cluster centre where both are statistically indistinguishable (e.g. Bonatto & Bica 2005, and references therein). Most of the cluster stars are contained within $R_{\rm RDP}$, which should not be mistaken for the tidal radius.[13] The cluster radii of the present objects are given in angular and absolute scales (Table 2).

The density contrast parameter $\delta_{\rm c} = 1 + \sigma_0/\sigma_{\rm bg}$, which is relatively high ($3.5 < \delta_{\rm c} < 9.2$) for the present RDPs, is also given in Table 2. Since $\delta_{\rm c}$ is measured in colour–magnitude-filtered (lower noise) RDPs, it is usually higher than the visual contrast produced by images (e.g. Fig. 1).

Taken at face value, the core radius of NGC 2244 (for the MS+PMS stars) $R_{\rm c} \sim 2.6$ pc would put it beyond the median value of the distribution derived for a sample of relatively nearby OCs by Piskunov et al. (2007). NGC 2239, on the other hand, falls on the low-$R_{\rm c}$ tail. Besides, assuming the relation tidal radius $\sim 2 \times R_{\rm RDP}$ (Bonatto & Bica 2005), both clusters fall around the median value of the tidal radius distribution.

6 CLUSTER MASS

Both clusters clearly present distinct populations of MS and PMS stars (Figs 6 and 7). As the first step to estimate the cluster masses, we build the LFs in the $K_{\rm s}$ band for the MS and PMS stars separately, by means of the respective colour–magnitude filters (Section 3.3). We show them in Fig. 12, where the similar age, different distances and number of members are reflected, especially on the different MS and PMS cut-offs. In both cases, the PMS LFs present the expected steep increase towards faint magnitudes (low-mass stars), which confirms that PMS stars are an important fraction of the members.

For a more objective investigation on the stellar mass distribution, we build the MFs [$\phi(m) = {\rm d}N/{\rm d}m$] for the current MS stars that, in turn, can be used to compute the mass stored in stars. Similarly to the RDPs (Section 5), we work with colour–magnitude filtered photometry to minimize noise. First, we build the LF independently for each 2MASS band, both for the cluster region ($R < R_{\rm RDP}$) and comparison field. The intrinsic LFs are obtained by subtracting the respective (equal area) comparison field LF from that of the cluster. The intrinsic LFs are transformed into MFs with the mass–luminosity relations obtained from the corresponding age and distance from the Sun solutions (Section 4). The final MF is produced by combining the J, H and $K_{\rm s}$ MFs into a single MF. Further details on MF construction are given in Bica, Bonatto & Blumberg (2006). The effective MS stellar mass ranges are $(4.6 \pm 2.2) \leq m(\mathrm{M}_\odot) \lesssim 60$ (NGC 2244) and $(3.2 \pm 0.5) \leq m(\mathrm{M}_\odot) \lesssim 14$ (NGC 2239). As Fig. 12 (bottom panels) shows, the MS MFs are rather smooth and present different lower and upper masses, which reflects the lower distance and younger age of NGC 2244 with respect to NGC 2239.

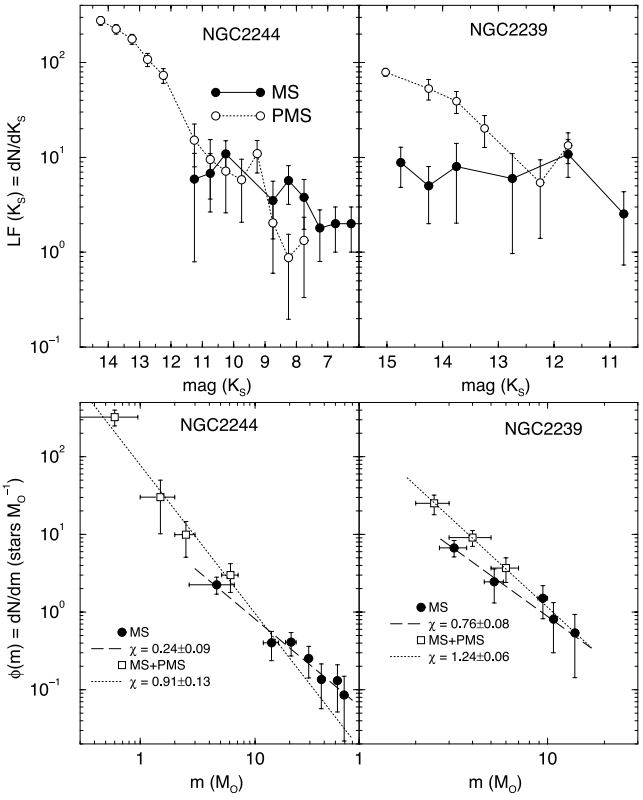

Figure 12. Top panels: $K_{\rm s}$-LFs of the MS (filled circles) and PMS (empty circles) stars. Bottom: MFs (for the J, H and $K_{\rm s}$ bands combined) of the MS (filled circles) and MS+PMS (empty squares). Fits of the function $\phi(m) \propto m^{-(1+\chi)}$ are shown by the dashed (MS) and dotted (MS+PMS) lines.

Since PMS stars are abundant in both clusters, it is important to build their MF as well. In Fig. 9 (right-hand panels), we show the evolutionary tracks (Siess et al. 2000) of PMS stars of different masses superimposed on the decontaminated CMDs of NGC 2244 and 2239. It is clear, especially for NGC 2244, that PMS stars less massive than $1\,\mathrm{M}_\odot$ are the most abundant component. Similarly to the MS, the PMS MFs are built with the number of PMS stars among any two tracks in the cluster region and comparison field. Finally, we add the MS and PMS MFs to produce the total MF of each cluster (Fig. 12).

The number of MS ($n_{\rm MS}$) and PMS ($n_{\rm PMS}$) members in NGC 2244 (for $R \leq R_{\rm RDP}$) are derived by counting the stars in the background-subtracted colour–magnitude filtered photometry. We apply the same approach as above to compute the PMS mass. There are $n_{\rm MS} = 26 \pm 3$ and $n_{\rm PMS} = 301 \pm 60$ stars; the corresponding mass values are $m_{\rm MS} = 389 \pm 44\,\mathrm{M}_\odot$ and $m_{\rm PMS} = 236 \pm 46\,\mathrm{M}_\odot$ (computed assuming the average mass between any two evolutionary tracks in Fig. 9). Thus, the total stellar mass of NGC 2244 is $m_{\rm MS+PMS} \approx 625\,\mathrm{M}_\odot$, which agrees with the $770\,\mathrm{M}_\odot$ mass estimated by Pérez (1991). We note that this value is about 10 per cent of the mass estimated by Ogura & Ishida (1981) for NGC 2244. However, this difference may arise from the present detailed

[13] Tidal radii are derived from, for example the three-parameter King-profile fit to RDPs (Bonatto & Bica 2008), which requires large surrounding fields and adequate errors. For instance, in populous and relatively high Galactic latitude OCs such as M 67, NGC 188 and 2477, the tidal radii are a factor of $\sim$2 larger than $R_{\rm RDP}$ (Bonatto & Bica 2005).

analysis - especially, the decontamination and the separation of MS and PMS stars in the construction of the cluster MF. The same analysis applied to NGC 2239 yields $n_{\rm MS} = 26 \pm 3$, $n_{\rm PMS} = 70 \pm 11$, $m_{\rm MS} = 141 \pm 16\,{\rm M}_\odot$, $m_{\rm PMS} = 160 \pm 32\,{\rm M}_\odot$ and the total stellar mass $m_{\rm MS+PMS} \approx 301\,{\rm M}_\odot$, about half the mass of NGC 2244.

Considering the MS stars isolately, the MFs can be well represented by the function $\phi(m) \propto m^{-(1+\chi)}$, with the slopes $\chi = 0.24 \pm 0.09$ and $\chi = 0.76 \pm 0.08$, respectively, for NGC 2244 and 2239. Both values are flatter than the $\chi = 1.35$ of Salpeter (1955) IMF. A flat MF slope was also found for NGC 2244 by Park & Sung (2002). However, when the MS and PMS stars are taken together, the slopes become steeper, $\chi = 0.91 \pm 0.13$ and 1.24 ± 0.06. While within uncertainties the total MF of NGC 2239 is comparable to the Salpeter (1955) IMF, the MF of NGC 2244 remains somewhat flatter, but still consistent with the conclusions of Wang et al. (2008).

7 DISCUSSION

Constrained by isochrone fits (Section 4), we could derive fundamental and structural parameters of the young OCs NGC 2244 and 2239, part of them for the first time. We use them to compare some of their properties with those of well-studied OCs.

7.1 Diagnostic diagrams

We further investigate the nature of NGC 2244 and 2239 with diagrams that examine relations among astrophysical parameters of OCs in different environments. They were introduced by Bonatto & Bica (2005). As reference sample we use some bright nearby OCs (Bonatto & Bica 2005; Bonatto et al. 2006b), and a group of OCs projected towards the central parts of the Galaxy (Bonatto & Bica 2007a). Also included are the young OCs NGC 6611 with the age ∼1.3 Myr (Bonatto et al. 2006c), NGC 6823 with ∼4 Myr and Bochum 1 with ∼9 Myr (Bica et al. 2008b). NGC 6611 and 6823 serve as comparison with gravitationally bound objects of similar age, while Bochum 1 is a star cluster fossil remain that might be dynamically evolving into an OB association. The full sample of comparison OCs is characterized by ages in the range ∼1.3 Myr to ∼7 Gyr, and Galactocentric distances within $5.8 \lesssim R_{\rm GC}({\rm kpc}) \lesssim 8.1$. Their parameters have been obtained following the same prescriptions as those for NGC 2244 and 2239.

The diagrams are shown in Fig. 13, where panels (a) and (b) examine the dependence of cluster ($R_{\rm RDP}$) and core ($R_{\rm c}$) radii on cluster age, respectively. Most of the small-radius OCs (especially in $R_{\rm RDP}$) occur at an age of ∼0.5–1 Gyr, the typical time-scale of OC disruption processes near the solar circle (e.g. Bergond, Leon & Guilbert 2001; Lamers et al. 2005). Both NGC 2244 and 2239 present a cluster radius comparable to that of NGC 6611 (and in general equivalent to other young OCs). The same applies to the core radius of NGC 2239. NGC 2244, on the other hand, has an $R_{\rm c}$ too large when compared to the reference OCs.

Core and cluster radii of the reference OCs follow the relation $R_{\rm RDP} = (8.9 \pm 0.3) \times R_{\rm C}^{(1.0\pm0.1)}$ (panel c),[14] suggesting a similar scaling for both kinds of radii. While NGC 2239 fits tightly in that relation, NGC 2244 deviates again probably because of the exceeding cluster radius. A dependence of OC size on Galactocentric distance is suggested by panel (d), as discussed by Lyngå (1982) and Tadross et al. (2002). While NGC 2244 follows the trend, NGC 2239 deviates somewhat. This relation may be partly primordial, in the sense that the high molecular gas density in central Galactic regions may have produced small clusters (e.g. van den Bergh, Morbey & Pazder 1991). After formation, mass loss due to stellar and dynamical evolution (e.g. mass segregation and evaporation), together with tidal interactions with the Galactic potential and giant molecular clouds, also contribute to the depletion of star clusters, especially the low mass and centrally located ones.

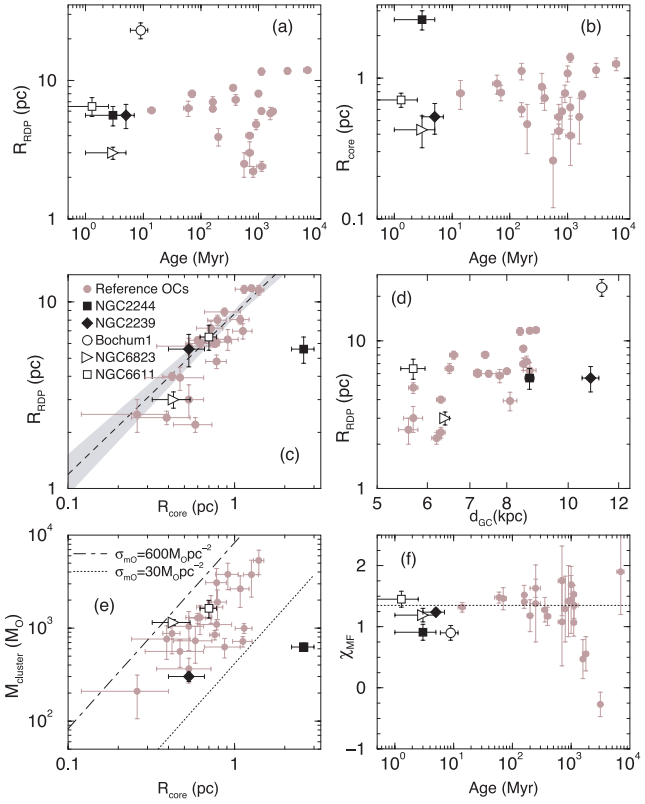

Figure 13. Diagrams dealing with astrophysical parameters of OCs. Gray-shaded circles: reference OCs. The young star clusters NGC 6611, 6823 and Bochum 1 are indicated for comparison purposes. Analytical relations in panels (c) and (e) are discussed in the text. Dotted line in panel (f) shows Salpeter (1955) IMF slope $\chi = 1.35$.

When the mass–density radial distribution follows a King-like profile (e.g. Bonatto & Bica 2007b, 2008; Bonatto, Bica & Santos 2008), the cluster mass inside $R_{\rm RDP}$ can be computed as a function of the core radius ($R_{\rm c}$) and the central mass-surface density (σ_{M0}), $M_{\rm clus} = \pi\, R_{\rm C}^2 \sigma_{\rm M0}\, \ln[1+(R_{\rm RDP}/R_{\rm c})^2]$. With the above relation (panel c) between $R_{\rm c}$ and $R_{\rm RDP}$, this equation becomes $M_{\rm clus} \approx 13.8 \sigma_{\rm M0}\, R_{\rm C}^2$. The observed relation of core radius and cluster mass is examined in panel (e). The reference OCs, together with NGC 2239 are contained within King-like distributions with central mass densities within $30 \lesssim \sigma_{M0}({\rm M}_\odot\,{\rm pc}^{-2}) \lesssim 600$. NGC 2244 appears to have too big a core radius for its total mass.

Finally, when the total (MS+PMS) MF slope is considered (panel f), NGC 2239 and especially NGC 2244 appear to have MFs flatter than those of similarly young OCs. On the other hand, their slopes are equivalent to those derived for some old OCs in the reference sample. In general, flat MFs reflect advanced dynamical evolution (e.g. Bonatto & Bica 2005).

What follows from the above analysis is that while NGC 2239 appears to be characterized by parameters of a typical young OC,

[14] Similar relations were also found by Nilakshi, Pandey & Mohan (2002), Sharma et al. (2006) and Maciejewski & Niedzielski (2007).

NGC 2244, on the other hand, exhibits evidence of a system far from dynamical equilibrium, which agrees with Chen et al. (2007) and Wang et al. (2008).

8 SUMMARY AND CONCLUSIONS

In the present paper, we employ the wide-field and NIR depth provided by 2MASS to focus on the Rosette Nebula cluster NGC 2244 and the nearby projected OC NGC 2239. Our approach relies essentially on field-star decontaminated 2MASS photometry, which enhances cluster CMD evolutionary sequences and stellar RDPs, producing more constrained fundamental and structural parameters.

Previous studies were mostly based on optical photometry and/or NIR with small angular fields. However, 2MASS can still provide additional insight (Section 3). The set of tools developed by our group allowed to unambiguously isolate MS and PMS stars that, in turn, resulted in well-defined CMDs, RDPs and MFs. In addition, we explore PM properties to investigate the other cluster in the area, NGC 2239.

Taken together, the (decontaminated) MS and PMS sequences of NGC 2244 provided an age range 1–6 Myr, an absorption $A_V = 1.7 \pm 0.2$ and a distance from the Sun $d_\odot = 1.6 \pm 0.2$ kpc ($\approx$1.5 kpc outside the solar circle). These parameters are consistent with most of the previous estimates. The (MS+PMS) MF slope $\chi = 0.91 \pm 0.13$ is somewhat flatter than the Salpeter (1955) IMF. With a total (MS+PMS) stellar mass of $m_{\rm MS+PMS} \sim 625\,{\rm M}_\odot$ derived in the present work, NGC 2244 is not as massive as previously estimated (Section 2). The King-like profile fit to the (MS+PMS) stellar RDP was obtained with a core radius $R_{\rm c} \approx 5.6$ arcmin ≈ 2.6 pc; the corresponding cluster radius is $R_{\rm RDP} \approx 10$ arcmin ≈ 4.7 pc. Compared to a set of well-known OCs, the core radius of NGC 2244 appears to be abnormally big, which puts it at unusual loci in the structural/dynamical diagnostic diagrams (Section 7.1). NGC 2244 has a central cusp that cannot be fitted by for example a King's law. This cusp is probably due to a star-formation effect, and not the product of dynamical evolution. We conclude that NGC 2244 is not in dynamical equilibrium, consistent with Chen et al. (2007) and Wang et al. (2008).

NGC 2239 is a low-mass ($m_{\rm MS+PMS} \approx 301\,{\rm M}_\odot$), young ($5 \pm 4$ Myr) and somewhat more absorbed ($A_V = 3.4 \pm 0.2$) OC, at $d_\odot = 3.9 \pm 0.4$ kpc, thus in the background of NGC 2244. Structurally, its RDP can be represented by a King-like profile with $R_{\rm c} \approx 0.5$ arcmin ≈ 0.5 pc and $R_{\rm RDP} \approx 5.0$ arcmin ≈ 5.6 pc. With $\chi = 1.24 \pm 0.06$, its composite MS+PMS MF slope is essentially Salpeter's IMF. These parameters characterize an average young OC, as compared to the reference nearby OCs (Section 7.1).

While NGC 2239 is a *normal* young OC with MS and PMS stars distributed according to a cluster RDP, NGC 2244 appears to be another example, like Bochum 1 (Bica et al. 2008b), of an OC doomed to dissolution in a few 10^7 yr. The present work shows the importance of field-star decontamination and wide-field extractions to get the best stellar statistics and to produce high-quality CMDs and RDPs.

ACKNOWLEDGMENTS

We thank the referee, Dr. M. Pérez, for comments. We acknowledge support from the Brazilian Institution CNPq. This publication makes use of data products from the 2MASS, which is a joint project of the University of Massachusetts and the Infrared Processing and Analysis Centre/California Institute of Technology, funded by the National Aeronautics and Space Administration and the National Science Foundation. This research has made use of the WEBDA data base, operated at the Institute for Astronomy of the University of Vienna.

REFERENCES

Alessi B. S., Moitinho A., Dias W. S., 2003, A&A, 410, 565
Berghöfer T. W., Christian D. J., 2002, A&A, 384, 890
Bergond G., Leon S., Guilbert J., 2001, A&A, 377, 462
Bessel M. S., Brett J. M., 1988, PASP, 100, 1134
Bica E., Bonatto C., 2008, MNRAS, 384, 1733
Bica E., Bonatto C., Barbuy B., Ortolani S., 2006, A&A, 450, 105
Bica E., Bonatto C., Blumberg R., 2006, A&A, 460, 83
Bica E., Bonatto C., Camargo D., 2008a, MNRAS, 385, 349
Bica E., Bonatto C., Dutra C., 2008b, A&A, 489, 1129
Binney J., Merrifield M., 1998, Galactic Astronomy. Princeton Series in Astrophysics. Princeton Univ. Press, Princeton
Bonatto C., Bica E., 2003, A&A, 405, 525
Bonatto C., Bica E., 2005, A&A, 437, 483
Bonatto C., Bica E., 2006, A&A, 455, 931
Bonatto C., Bica E., 2007a, MNRAS, 377, 1301
Bonatto C., Bica E., 2007b, A&A, 473, 445
Bonatto C., Bica E., 2008, A&A, 477, 829
Bonatto C., Bica E., 2009, MNRAS, 392, 483
Bonatto C., Bica E., Girardi L., 2004, A&A, 415, 571
Bonatto C., Bica E., Santos Jr J. F. C., 2005, A&A, 433, 917
Bonatto C., Kerber L. O., Bica E., Santiago B. X., 2006a, A&A, 446, 121
Bonatto C., Bica E., Ortolani S., Barbuy B., 2006b, A&A, 453, 121
Bonatto C., Santos Jr J. F. C., Bica E., 2006c, A&A, 445, 567
Bonatto C., Bica E., Santos Jr J. F. C., 2008, MNRAS, 386, 324
Cardelli J. A., Clayton G. C., Mathis J. S., 1989, ApJ, 345, 245
Chen L., de Grijs R., Zhao J. L., 2007, AJ, 134, 1368
Dutra C. M., Santiago B. X., Bica E., 2002, A&A, 383, 219
Eisenhauer F., Schödel R G. R., Ott T., Tecza M., Abuter R., Eckart A., Alexander T., 2003, ApJ, 597, L121
Eisenhauer F. et al., 2005, ApJ, 628, 246
Elson R. A. W., Fall S. M., Freeman K. C., 1987, ApJ, 323, 54
Friel E. D., 1995, ARA&A 1995, 33, 381
Girardi L., Bertelli G., Bressan A., Chiosi C., Groenewegen M. A. T., Marigo P., Salasnich B., Weiss A., 2002, A&A, 391, 195
Goodwin S. P., Bastian N., 2006, MNRAS, 373, 752
Hensberge H., Pavlovski K., Verschueren W., 2000, in Favata F., Kaas A., Wilson A., eds, ESLAB Symp. 33. Star Formation from the Small to the Large Scale. ESA, Noordwijk
Hurley J., Tout A. A., 1998, MNRAS, 300, 977
Kerber L. O., Santiago B. X., Castro R., Valls-Gabaud D., 2002, A&A, 390, 121
King I., 1962, AJ, 67, 471
King I., 1966, AJ, 71, 64
Lada C. J., Lada E. A., 2003, ARA&A, 41, 57
Lamers H. J. G. L. M., Gieles M., Bastian N., Baumgardt H., Kharchenko N. V., Portegies Zwart S., 2005, A&A, 441, 117
Li J. Z., 2005, ApJ, 625, 242
Lyngå G., 1982, A&A, 109, 213
Maciejewski G., Niedzielski A., 2007, A&A, 467, 1065
Mercer E. P. et al., 2005, ApJ, 635, 560
Naylor T., Jeffries R. D., 2006, MNRAS, 373, 1251
Nilakshi S. R., Pandey A. K., Mohan V., 2002, A&A, 383, 153
Nishiyama S. et al., 2006, ApJ, 647, 1093
Ogura K., Ishida K., 1981, PASJ, 33, 149
Park B.-G., Sung H., 2002, AJ, 123, 892
Pérez M. R., 1991, RMxAA, 22, 99
Pérez M. R., Thé P. S., Westerlund B. E., 1987, PASP, 99, 1050
Phelps R. L., Lada E. A., 1997, ApJ, 477, 176
Piskunov A. E., Schilbach E., Kharchenko N. V., Röser S., Scholz R.-D., 2007, A&A, 468, 151

Richer H. B. et al., 2008, AJ, 135, 2141
Román-Zúñiga C. G., Lada E. A., 2008, in Bo Reipurth, ed., ASP Conf. Ser. Vol., Handbook of Star Forming Regions, Vol. I: The Northern Hemisphere. Astron Soc. Pac., San Francisco
Salpeter E., 1955, ApJ, 121, 161
Sharma S., Pandey A. K., Ogura K., Mito H., Tarusawa K., Sagar R., 2006, AJ, 132, 1669
Siess L., Dufour E., Forestini M., 2000, A&A, 358, 593
Skrutskie M. et al., 1997, in Garzon F., Epchtein N., Omont A., Burton W. B., Persi P., eds, The Impact of Large Scale Near-IR Sky Surveys, Vol. 210. Kluwer, Dordrecht, p. 25
Sulentic J. W., Tifft W. G., 1973, The Revised New Catalogue of Nonstellar Astronomical Objects. University of Arizona Press, Tucson
Tadross A. L., Werner P., Osman A., Marie M., 2002, New Astron., 7, 553
Trager S. C., King I. R., Djorgovski S., 1995, AJ, 109, 218
van den Bergh S., Morbey C., Pazder J., 1991, ApJ, 375, 594
Wang J., Townsley L. K., Feigelson E. D., Broos P. S., Getman K. V., Román-Zúñiga C. G., Lada E., 2008, ApJ, 675, 464
Wilson C. P., 1975, AJ, 80, 175

This paper has been typeset from a TEX/LATEX file prepared by the author.